

# Third-order phase transition in random tilings

F. Colomo and A. G. Pronko

ABSTRACT. We consider the domino tilings of an Aztec diamond with a cut-off corner of macroscopic square shape and given size, and address the bulk properties of tilings as the size is varied. We observe that the free energy exhibits a third-order phase transition when the cut-off square, increasing in size, reaches the arctic ellipse—the phase separation curve of the original (unmodified) Aztec diamond. We obtain this result by studying the thermodynamic limit of certain nonlocal correlation function of the underlying six-vertex model with domain wall boundary conditions, the so-called emptiness formation probability (EFP). We consider EFP in two different representations: as a tau-function for Toda chains and as a random matrix model integral. The latter has a discrete measure and a linear potential with hard walls; the observed phase transition shares properties with both Gross-Witten-Wadia and Douglas-Kazakov phase transitions.

## 1. Introduction

Dimer coverings and random tilings of regular lattices are problems of great and long-lasting interest [1–5]. In spite of the simplicity of their formulation, they exhibit numerous fascinating features. In particular, the dependence of macroscopic quantities (such as the free energy) on boundary conditions is most unusual and intriguing. For some recent advances on physics of dimers and related tiling problems and their applications see, e.g., [6, 7] and references therein.

The influence of boundary conditions on macroscopic quantities is related with the fact that random tiling of finite planar regions may exhibit phase separation phenomena. A famous example is provided by the domino tilings of the “Aztec diamond”, that exhibits “frozen” domino configurations in the corners, outside a central region of disorder; the phase separation curve emerging in the scaling limit is called arctic circle, or arctic ellipse for a weighted counting of configurations [8] (for recent developments, see, e.g., [9] and references therein). Another famous example is given by lozenges (rhombi) tilings of an hexagon, which are equivalent to boxed plane partitions [10]. In rather general settings these and other similar problems in mathematical literature are usually treated in terms of dimer models on planar bipartite graphs [11–13].

The phase separation phenomena can also be observed in vertex models, which can be treated as models of interacting dimers [14]. Most impressive results on this topic so far have been provided by numerical experiments [15, 16]. Some exact

analytical results for the six-vertex model were obtained in [17–19]; to progress further on this problem additional studies of random tilings seem to be very relevant.

In dealing with tiling problems one may wonder how stable are the observed bulk properties of tilings, such as free energy, phase separation phenomena, etc, against various deformations of the considered finite region. While it is clear that preserving a peculiar microscopic shape of the boundary of the region (e.g., the staircase shape for the boundary of the Aztec diamond) is crucial for obtaining the phase separation, one can also consider macroscopic transformations of the shape of the region.

The purpose of the present paper is to address this problem on the example of domino tilings. Specifically, we consider here the domino tilings of the Aztec diamond with a cut-off corner of macroscopic square shape and given size, and study the bulk properties of the tilings as the size is varied. We rely on the well-known correspondence between the domino tilings of the Aztec diamond and the six-vertex model with domain wall boundary conditions (DWBC) [20, 21]. Here we extend this correspondence to the domino tilings of the Aztec diamond with a cut-off corner. In this case, the six-vertex model is considered with a square portion of the lattice removed, but again with DWBC.

The partition function of the six-vertex model on this modified lattice can be written as certain nonlocal correlation function of the six-vertex model on the original lattice. This correlation function is exactly what is known as the emptiness formation probability (EFP), which can be viewed as a test function for total ferroelectric order in a rectangular subregion in a corner of the original lattice. Here we specialize the subregion to a square, and derive the behavior of EFP in the thermodynamic limit.

Restating the result in terms of tilings, we get the free energy of the domino tilings of the Aztec diamond with a cut-off corner, as a function of the size of the cut-off square. We observe that the free energy exhibits a third-order phase transition when the cut-off square, increasing in size, reaches the phase separation curve of the original (unmodified) Aztec diamond, the arctic ellipse.

This result provides a novel insight on the phase separation phenomena in tiling models. The phase separation curves can be seen as critical curves in the space of parameters describing the macroscopic geometry of the tiled region. While here we provide just a single example of this interpretation, focusing on the domino tilings of Aztec diamond, it may have rather universal nature and be observed in other tiling problems and dimer models.

We organize the paper as follows. In the next section we discuss the relation between tilings of the Aztec diamond with a cut-off square and EFP in the six-vertex model. In Section 3 we discuss a Hankel determinant formula for EFP, which can be viewed both as a solution of Toda chain differential equations, and as a random matrix model integral (with a discrete measure). In Section 4 we derive the result using the differential equations approach. In Section 5 we show how the same result can be obtained from the random matrix model integral. In Section 6 we discuss the connection of the observed phase transition with the arctic ellipse.

## 2. Domino tilings and the six-vertex model

First, recall (see [21]) that domino tilings can be formulated in terms of the six-vertex model on a square lattice by mapping elementary patches of domino tilings

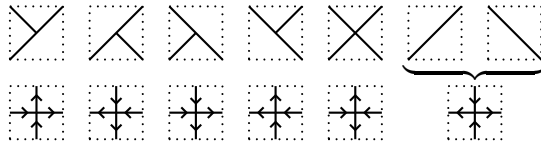


FIGURE 1. Elementary patches of domino tilings (top) and the corresponding configurations of the six-vertex model (bottom).

to arrow configurations as shown on Figure 1. The Aztec diamond of order  $N$  then corresponds to the six-vertex model on an  $N \times N$  lattice with a specific choice of arrows on the boundary edges, known as the DWBC [20], see Figure 2, picture on the left. As a dimer model on a bipartite graph, domino tilings of the Aztec diamond correspond to the coverings of a square portion of a fishnet-like square lattice, see Figure 2, picture on the right. Obviously, the results below thus apply not only to tilings but also to dimers.

Let  $w_i$  denote the Boltzmann weight of the  $i$ th arrow configuration around a vertex,  $i = 1, \dots, 6$ , as they appear on Figure 1 from left to right. The plain enumerations of domino tilings correspond to the choice  $w_1 = \dots = w_5 = 1$  and  $w_6 = 2$ . More generally, one may consider  $w_i$ 's arbitrary but obeying the free-fermion condition,

$$w_1 w_2 + w_3 w_4 = w_5 w_6. \quad (2.1)$$

The partition function of the six-vertex model with DWBC on the  $N \times N$  lattice,  $Z_N$ , for weights satisfying the condition (2.1), has an extremely concise form (see, e.g., [21]):

$$Z_N = w_5^{\frac{N(N-1)}{2}} w_6^{\frac{N(N+1)}{2}}. \quad (2.2)$$

We shall use the following parameterization:

$$w_1 = w_2 = \sqrt{\rho(1-\alpha)}, \quad w_3 = w_4 = \sqrt{\rho\alpha}, \quad w_5 = 1, \quad w_6 = \rho. \quad (2.3)$$

Since in any configuration of the six-vertex model with DWBC the number of vertices of type 6 is equal to the number of vertices of type 5 plus  $N$ , the parameter  $\rho$  is just an overall normalization of weights. In the enumeration of domino tilings in terms of the six-vertex model configurations  $\rho = 2$ . On the contrary, the parameter  $\alpha$  is relevant. In the domino tilings it describes the asymmetry between the two orientations, namely NE-SW and NW-SE, of dominoes, giving them the weights  $\sqrt{2(1-\alpha)}$  and  $\sqrt{2\alpha}$ , respectively, in their weighted (“biased”) counting [8].

We now introduce the Aztec diamond with a cut-off corner. Given an Aztec diamond of order  $N = r + s$ , let us consider a new region which can be obtained from the original Aztec diamond by removing the dashed subregion indicated in Figure 3. This subregion can be viewed as an Aztec diamond of order  $s$ , with one NE-SW row deleted in the middle, and it admits only one tiling, with all dominoes NE-SW oriented. The new region<sup>1</sup> thus obtained is the Aztec diamond with a cut-off corner. We note that it can be tiled with dominoes only for  $s \leq r$ , as it can be easily seen in the dimer context.

The Aztec diamond with a cut-off corner can be related to the six-vertex model in standard way. The six-vertex model is now defined on an  $(r + s) \times (r + s)$  lattice

<sup>1</sup>Note that the new region must contain a line segment attached to the SE corner of the removed subregion, to keep connection with the six-vertex model.

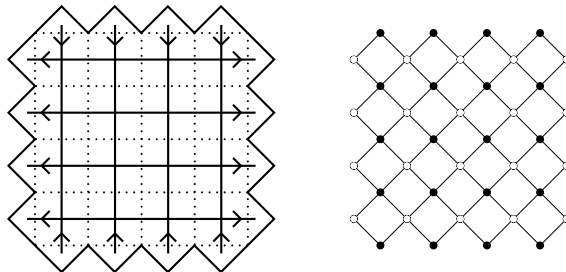


FIGURE 2. An Aztec diamond of order  $N$  and the underlying  $N \times N$  square lattice with DWBC,  $N = 4$  (left); the bipartite graph for the related dimer model (right).

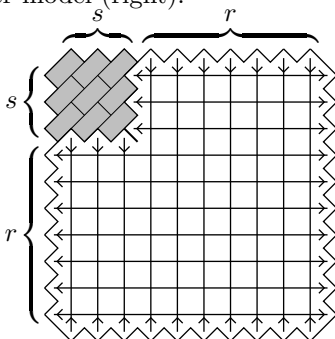


FIGURE 3. The Aztec diamond of order  $r+s$ , with a cut-off square of size  $s$ , and the corresponding lattice for the six-vertex model,  $r = 7$ ,  $s = 3$ .

with a square portion of the lattice, of size  $s$ , removed. Due to the relation between dominoes and vertex configurations (Figure 1), the six-vertex model with a cut-off square must have again DWBC, namely all horizontal external arrows are outgoing, and all vertical ones are incoming, for the new boundary edges as well, as shown in Figure 3. We denote the partition function of the six-vertex model on the new lattice as  $Z_{r,s}$ .

We are interested in the thermodynamic limit of large lattices, with large sizes of the cut-off corner. We thus consider both  $r$  and  $s$  large, with the ratio  $s/r =: v$  fixed. Since the model is meaningful only for  $s \leq r$ , variable  $v$  runs over the interval  $[0, 1]$ . We define the free energy per site of the six-vertex model with a cut-off corner by

$$F(v) = - \lim_{\substack{r,s \rightarrow \infty \\ s/r=v}} \frac{\log Z_{r,s}}{r^2 + 2rs}. \quad (2.4)$$

Clearly,  $F(v)$  is also the free energy per domino for domino tilings of a large Aztec diamond (of order  $r(1+v)$ ,  $r \rightarrow \infty$ ) with a cut-off corner of square shape (and size  $rv$ ).

To evaluate the partition function  $Z_{r,s}$ , let us now introduce EFP, a nonlocal correlation function of the six-vertex model on the complete lattice [22]. This correlation function, denoted  $f_{r,s}$ , can be defined as the probability that the vertices of the  $s \times s$  subregion at the top-left corner of the  $(r+s) \times (r+s)$  lattice with

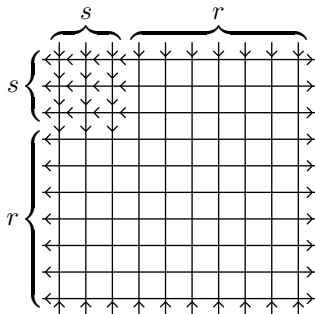


FIGURE 4. The configuration of arrows whose probability is equal to  $f_{r,s}$ .

DWBC are all of type 2, see Figure 4. Note, that the definition of EFP can be easily extended to a more general situation where the subregion at top-left corner has a rectangular shape; here we consider only the case of a square shape.

It is clear that EFP coincides, modulo a simple overall factor, with the partition function of the six-vertex model on the same  $(r + s) \times (r + s)$  lattice but with all the vertices belonging to the  $s \times s$  subregion in the top-left corner lattice removed, see Figure 3. Indeed, for general values of the six-vertex model weights (i.e. not only under the condition (2.1)), we may write

$$Z_{r,s} = \frac{Z_{r+s}}{(w_2)^{s^2}} f_{r,s}. \tag{2.5}$$

with the convention that  $Z_{r,0} = Z_r$ .

Given the above definition of EFP, one can compute it for some special cases. First we note that the set of admissible configurations is empty for  $s$  greater than  $r$ , so that EFP is nontrivial only for  $s = 0, 1, \dots, r$ . Aside from the obvious case of  $s = 0$ , in which

$$f_{r,0} = 1, \tag{2.6}$$

there are two other easily computable cases, namely  $s = 1$  and  $s = r$ . In the first case EFP can be inferred from the observation that the probability of having a vertex of type 2 at the very top-left corner of the lattice is equal to one, minus the probability of having the vertex of type 6 (see Figure 1, and also discussion in [23]), hence

$$f_{r,1} = 1 - \frac{w_6(w_3w_4)^r Z_r}{Z_{r+1}} = 1 - \alpha^r. \tag{2.7}$$

In the second case,  $r = s$ , the  $2r \times 2r$  lattice splits onto four  $r \times r$  sublattices; all vertices of the top-left sublattice are of type 2, of the bottom-right one are of type 1, and the top-right and the bottom-left sublattices have DWBC, hence

$$f_{r,r} = \frac{(w_1w_2)^{r^2} Z_r^2}{Z_{2r}} = (1 - \alpha)^{r^2}. \tag{2.8}$$

Note that (2.6) and the first equalities in (2.7) and (2.8) hold for generic weights, independently of the free-fermion condition (2.1).

In the thermodynamic limit, where both  $r$  and  $s$  are large, with the ratio  $v = s/r$  fixed,  $v \in [0, 1]$ , EFP can be described by function  $\sigma(v)$ , defined by

$$f_{r,s} = \exp \{ -r^2 \sigma(s/r) + o(r^2) \}, \quad s, r \rightarrow \infty. \quad (2.9)$$

Some properties of the function  $\sigma(v)$  can be seen directly from the definition of the EFP. For instance,  $f_{r,s}$  being a probability, it varies from 0 to 1, and thus  $\sigma(v) \geq 0$ . Furthermore, since increasing the ratio  $s/r = v$  corresponds to decreasing the number of configurations contributing into the EFP, it follows that  $\sigma(v)$  is a nondecreasing function of its variable.

From (2.3) and (2.5), we may write the free energy per site (2.4) of the six-vertex model with a cut-off corner as

$$F(v) = -\log \sqrt{\rho} + \frac{v^2}{1+2v} \log \sqrt{1-\alpha} + \frac{1}{1+2v} \sigma(v). \quad (2.10)$$

Thus the free energy density  $F(v)$  is completely determined by the function  $\sigma(v)$ , which is the object of our study in what follows.

Before addressing the exact form of the function  $\sigma(v)$ , let us discuss its behaviour qualitatively. We recall that the arctic circle (or, in general, ellipse) phenomenon in the domino tilings of the Aztec diamond is the emergence, in the thermodynamic limit, of four frozen regions in the corners, sharply separated from a central region of disorder.

Turning to the language of the six-vertex model, this implies in particular the presence of a frozen region of vertices of type 2 in the top-left corner, outside the arctic ellipse. Thus, by construction (see also discussion in [24]), EFP must tend to one, as the lattice coordinates  $r$  and  $s$  get large,  $r, s \rightarrow \infty$ , but such that the corresponding  $s \times s$  subregion is entirely contained in the top-left frozen region, i.e., outside of the arctic ellipse. For the same reason, EFP is expected to tend to zero, as  $r, s \rightarrow \infty$  and such that the  $s \times s$  subregion in the top-left corner overlaps with the central region of disorder.

In view of this behavior, it is quite naturally to expect that the function  $\sigma(v)$ , defined in (2.9), vanishes identically on some interval  $[0, v_c]$ , where the value of  $v_c$  corresponds to the arctic ellipse. On the remaining interval, i.e., for  $v \in [v_c, 1]$ , the function  $\sigma(v)$  is expected to be positive-valued and nondecreasing function of  $v$ . This is indeed what we shall observe in the following by analysing some exact representation for EFP. Further discussion in connection with the arctic ellipse phenomenon is given in Section 6.

### 3. EFP as a Hankel determinant

In this section we discuss our main tool to study EFP, namely, its representation in terms of certain Hankel determinant.

We first mention that in our previous works, our treatment of EFP in the six-vertex model with DWBC was based on certain representation in terms of a multiple integral, valid for the model with generic weights, and derived in [22]. In the special case of the free-fermion weights we used this representation to recover the arctic ellipse in [24]; the case of generic weights and the corresponding arctic curves were considered in [18, 19]. However, such representation turns out having rather limited capabilities to address the asymptotic properties of EFP in the thermodynamic limit, even in the technically simple case of the free-fermion model (see, e.g., the discussion in [24]).

Motivated by this problem, in [25] various alternative representations for EFP in the case of the free-fermion model were provided. The main result concerned a Hankel determinant formula, which can be viewed as resulting from the evaluation of all the integrals in the multiple integral representation. In the special case of EFP of a square shaped region, the Hankel determinant representation reads:

$$f_{r,s} = \frac{(1-\alpha)^{s^2}}{\left(\prod_{j=1}^{s-1} j!\right)^2 \alpha^{s(s-1)/2}} \det_{1 \leq j,k \leq s} \left[ \sum_{m=0}^{r-1} m^{j+k-2} \alpha^m \right]. \quad (3.1)$$

This representation allows one to relate EFP with a set of Toda chain differential equations and with a random matrix model possessing a simple potential.

A relation of (3.1) with Toda chains can be established due to its Hankel determinant structure, using the fact that all entries in the determinant can be obtained by acting with the differential operators  $(\alpha \partial_\alpha)^{j+k-2}$  on certain function of  $\alpha$ , independent of  $s$ . This allows one to use the Sylvester determinant identity to treat the determinant as the tau-function of some Toda chain [26, 27]. One can obtain the following equation for EFP:

$$(\alpha \partial_\alpha)^2 \log f_{r,s} = \frac{s^2 \alpha}{(1-\alpha)^2} \left( \frac{f_{r,s+1} f_{r,s-1}}{f_{r,s}^2} - 1 \right). \quad (3.2)$$

This equation, supplemented by values of  $f_{r,s}$  at  $s = 0$  and  $s = 1$ , given by (2.6) and (2.7), respectively, allows one to reconstruct the function  $f_{r,s}$  iteratively for the remaining values of  $s$ . In [25], it was also proven that, for any given  $s$ , the function  $f_{r,s}$  satisfies the following equation, where now  $r$  varies:

$$(\alpha \partial_\alpha)^2 \log f_{r,s} = \frac{r^2 \alpha}{(1-\alpha)^2} \left( \frac{f_{r+1,s} f_{r-1,s}}{f_{r,s}^2} - 1 \right). \quad (3.3)$$

The existence of this equation can be ascribed to the fact that EFP has one more representation, similar to (3.1), but now in terms of an  $(r-s) \times (r-s)$  determinant with entries depending on  $s$  (but not on  $r$ ); for further details, see [25], Section 3.

The Hankel determinant representation (3.1) can be easily related to random matrix models as well. Indeed, extracting the sums from the determinant, which takes the Vandermonde form, and symmetrizing the obtained expression, one gets

$$f_{r,s} = \frac{(1-\alpha)^{s^2}}{s! \left(\prod_{j=1}^{s-1} j!\right)^2 \alpha^{s(s-1)/2}} \sum_{m_1=0}^{r-1} \cdots \sum_{m_s=0}^{r-1} \prod_{j < k} (m_k - m_j)^2 \prod_{j=1}^s \alpha^{m_j}. \quad (3.4)$$

This expression can be viewed as the standard integral formula, although with a discrete measure, for a random matrix model partition function with a linear potential and two hard walls, see the discussion in Section 5. We mention that a similar expression appeared also in certain random growth model [28].

To derive the function  $\sigma(v)$  from the Hankel determinant representation, we shall need its values, at  $v = 0$  and  $v = 1$ , for the Toda differential equation approach, and as  $\alpha \rightarrow 0$  and  $\alpha \rightarrow 1$ , for the random matrix model approach. Some of these values directly follows from the definition of EFP, while other can be obtained only from an explicit evaluation of the Hankel determinant in (3.1).

First, we consider EFP in the case of large  $r$  and finite  $s$ . As explained in Appendix A, the Hankel determinant in (3.1) admits an explicit evaluation at  $r = \infty$ , for  $\alpha$  arbitrary. The result is given by (A.2). Since for large  $r$  every entry can

be represented as its value at  $r = \infty$ , minus an  $O(\alpha^r)$  term, we have an estimate of the form

$$\det_{1 \leq j < k \leq s} \left[ \sum_{m=0}^{r-1} m^{j+k-2} \alpha^m \right] = \prod_{j=0}^{s-1} \frac{(j!)^2 \alpha^j}{(1-\alpha)^{2j+1}} + O(\alpha^r). \quad (3.5)$$

In this estimate we assume that  $\alpha \in (0, 1)$ , i.e., we exclude the values  $\alpha = 0$  and  $\alpha = 1$  in the discussion of the large  $r$  limit,  $s$  finite. The formula above implies that EFP takes values close to one, up to exponentially small corrections,

$$1 - f_{r,s} = O(\alpha^r), \quad r \rightarrow \infty. \quad (3.6)$$

Such behavior in fact implies that at  $v = 0$  the function  $\sigma(v)$  vanishes together with all its derivatives,

$$\sigma^{(n)}(0) = 0, \quad n = 0, 1, \dots \quad (3.7)$$

Note that for  $n = 0, 1$  this could already be argued from (2.6) and (2.7).

Next we consider the case of  $s = r$ , at arbitrary  $\alpha$ . It can be easily seen that (3.1) immediately reproduces (2.8) by noting that the multiple sum in (3.4), modulo permutations, is given by a single term, with  $m_j = j - 1$ . Hence,

$$\sum_{m_1=0}^{r-1} \cdots \sum_{m_r=0}^{r-1} \prod_{j < k} (m_k - m_j)^2 \prod_{j=1}^r \alpha^{m_j} = r! \prod_{j=1}^{r-1} (j!)^2 \cdot \alpha^{r(r-1)/2}, \quad (3.8)$$

and in the thermodynamic limit we have

$$\sigma(1) = -\log(1 - \alpha), \quad (3.9)$$

which will be used together with (3.7) in the next section.

Let us now treat the case of  $\alpha \rightarrow 0$ , at arbitrary  $r$  and  $s$ . The result for EFP can be obtained directly from its definition, since the weights  $w_3$  and  $w_4$  vanish, and there is just a single configuration contributing to the partition function. We simply have

$$\lim_{\alpha \searrow 0} f_{r,s} = 1. \quad (3.10)$$

The same result is easily recovered from (3.4) by noting that, for small  $\alpha$ , only the term  $m_j = j - 1$  in the multiple sum (modulo permutations) is relevant, since all other terms are of higher order in  $\alpha$ , and (3.8) applies. In the thermodynamic limit we have

$$\lim_{\alpha \searrow 0} \sigma(v) = 0, \quad (3.11)$$

that will be used in the random matrix model approach in Section 5.

Finally, we study the case of  $\alpha \rightarrow 1$ . From the definition of EFP, recalling that in this case the weights  $w_1$  and  $w_2$  vanish, and that in each configuration these weights appear in pairs, it follows that

$$f_{r,s} \sim C_{r,s} (1 - \alpha)^{s^2}, \quad \alpha \rightarrow 1, \quad (3.12)$$

where  $C_{r,s}$  is some quantity independent of  $\alpha$ , which cannot be worked out simply by inspecting the configurations. However, one can find  $C_{r,s}$  from the Hankel determinant representation for EFP, since, as explained in Appendix A, the determinant in (3.1) at  $\alpha = 1$  can be explicitly evaluated, with the result given by (A.4).



Plugging it into (3.1) leads to (3.12) where the quantity  $C_{r,s}$  reads

$$C_{r,s} = \prod_{j=0}^{s-1} \frac{(j!)^2(j+r)!}{(2j)!(r-j-1)!(2j+1)!}. \quad (3.13)$$

In the thermodynamic limit, the quantity of interest being  $\sigma(v)$ , we may write

$$\lim_{\alpha \nearrow 1} [\sigma(v) + v^2 \log(1-\alpha)] = \psi(v), \quad (3.14)$$

where

$$\psi(v) := - \lim_{\substack{r,s \rightarrow \infty \\ s/r=v}} \frac{\log C_{r,s}}{r^2}. \quad (3.15)$$

From the exact expression (3.13) for the quantity  $C_{r,s}$ , using standard arguments based on Stirling formula, we easily obtain

$$\psi(v) = v^2 \log 4v - \frac{(1-v)^2}{2} \log(1-v) - \frac{(1+v)^2}{2} \log(1+v). \quad (3.16)$$

The function  $\psi(v)$  enters the derivation of the function  $\sigma(v)$  from the random matrix model integral.

#### 4. The differential equations approach

The approach which we intend to apply here to derive the function  $\sigma(v)$  is strongly inspired by that used in [27] where the partition function of the six-vertex model with DWBC was studied exploiting its property of being the tau-function of a semi-infinite Toda chain.

The derivation is based on the idea that (3.2) and (3.3) can be used to derive a set of partial differential equations for  $\sigma(v)$ . Indeed, substituting (the logarithm of) definition (2.9) into (3.2) and (3.3), replacing  $s$  with  $vr$ , dividing by  $r^2$ , and taking the limit  $r \rightarrow \infty$ , we obtain

$$\begin{aligned} (\alpha \partial_\alpha)^2 \sigma &= \frac{v^2 \alpha}{(1-\alpha)^2} \left(1 - e^{-\sigma''}\right), \\ (\alpha \partial_\alpha)^2 \sigma &= \frac{\alpha}{(1-\alpha)^2} \left(1 - e^{-v^2 \sigma'' + 2v\sigma' - 2\sigma}\right). \end{aligned} \quad (4.1)$$

Here the prime denotes the derivative with respect to  $v$  and to simplify writing we lift the dependence on  $v$ . The limit performed above holds uniformly in  $v$ , over any interval where  $\sigma''$  exists.

We first obtain solutions of the system of equations (4.1), and next explain how they can be used to construct the function  $\sigma(v)$  describing the thermodynamic limit of the EFP. Equating the right-hand sides of the two equations in (4.1) gives us the following ordinary differential equation in  $v$ :

$$v^2 e^{(v^2-1)\sigma'' - 2v\sigma' + 2\sigma} + (1-v^2) e^{v^2 \sigma'' - 2v\sigma' + 2\sigma} = 1. \quad (4.2)$$

Since both terms here in the left-hand side are nonnegative and vary from 0 to 1, we can parameterize them as  $\sin^2 \varphi$  and  $\cos^2 \varphi$ , respectively, with function  $\varphi = \varphi(v)$  taking values over the interval  $[0, \pi/2]$ . Thus we replace (4.2) by the system of two

equations for two functions,  $\sigma$  and  $\varphi$ ,

$$\begin{aligned}\sigma'' &= -2 \log \frac{\sin \varphi}{v} + 2 \log \frac{\cos \varphi}{\sqrt{1-v^2}}, \\ v\sigma' - \sigma &= -v^2 \log \frac{\sin \varphi}{v} - (1-v^2) \log \frac{\cos \varphi}{\sqrt{1-v^2}}.\end{aligned}\tag{4.3}$$

Since  $(v\sigma' - \sigma)' = v\sigma''$ , differentiating the second equation and subtracting the first one multiplied by  $v$  allows us to eliminate  $\sigma$  and to obtain the following equation for  $\varphi$ :

$$[(1-v^2) \tan \varphi - v^2 \cot \varphi] \varphi' = 0.\tag{4.4}$$

Obviously, this equation has two solutions, which we denote as  $\varphi_{\text{I}}$  and  $\varphi_{\text{II}}$ , which read

$$\varphi_{\text{I}}(v) = \arcsin v, \quad \varphi_{\text{II}}(v) = \omega,\tag{4.5}$$

where  $\omega$  is some function of  $\alpha$  (but not of  $v$ ).

Denoting by  $\sigma_{\text{I}}$  the solution of (4.3) that corresponds to  $\varphi_{\text{I}}$ , we find from (4.3) that it must satisfy the equations  $\sigma_{\text{I}}'' = v\sigma_{\text{I}}' - \sigma_{\text{I}} = 0$ . Hence, it is just a linear function in  $v$  of the form

$$\sigma_{\text{I}}(v) = Av,\tag{4.6}$$

where  $A$  depends on  $\alpha$ . To fix  $A$ , we plug this solution of (4.2) into (4.1) that gives us the equation  $(\alpha\partial_\alpha)^2 A = 0$ , which can be readily solved with the result

$$A = a_1 + a_2 \log \alpha,\tag{4.7}$$

where  $a_1$  and  $a_2$  are arbitrary constants.

The solution  $\sigma_{\text{II}}$  of (4.3) that corresponds to  $\varphi_{\text{II}}$  can be worked out in a similar manner. Solving (4.3) with  $\varphi$  replaced by a  $v$ -independent function  $\omega$ , we find the expression

$$\begin{aligned}\sigma_{\text{II}}(v) &= v^2 \log v - \frac{(1-v)^2}{2} \log(1-v) - \frac{(1+v)^2}{2} \log(1+v) \\ &\quad + v^2 \log \cot \omega + Bv + \log \cos \omega,\end{aligned}\tag{4.8}$$

where  $B$  depends on  $\alpha$ . We can find  $B$  and  $\omega$  by substituting the obtained solution into one of the two equations in (4.1). The resulting equation has in both sides second order polynomials in  $v$ ; matching terms in powers of  $v$  we obtain three ordinary differential equations in  $\alpha$ . The equation due to the first order term in  $v$  is  $(\alpha\partial_\alpha)^2 B = 0$ , from which we conclude that

$$B = b_1 + b_2 \log \alpha,\tag{4.9}$$

where  $b_1$  and  $b_2$  are some constants. The remaining two equations, due to the zeroth and second order terms in  $v$ , are

$$(\alpha\partial_\alpha)^2 \log \cos \omega = -\frac{\alpha}{(1-\alpha)^2} \tan^2 \omega\tag{4.10}$$

and

$$(\alpha\partial_\alpha)^2 \log \cot \omega = \frac{\alpha}{(1-\alpha)^2} \frac{1}{\cos^2 \omega},\tag{4.11}$$

respectively. Solving these equations and choosing the compatible solution, which additionally satisfies the condition to be a real-valued function of  $\alpha$  taking values

in the interval  $[0, \pi/2]$ , we obtain that

$$\omega = \arcsin u, \quad u := \frac{1 - \sqrt{\alpha}}{1 + \sqrt{\alpha}}. \quad (4.12)$$

This completes the construction of the solutions of the system of equations (4.1).

Let us now establish the form of the function  $\sigma(v)$  describing the thermodynamic limit of the EFP. First of all we note that the function  $\sigma(v)$  cannot be expressed in terms of either  $\sigma_{\text{I}}(v)$  or  $\sigma_{\text{II}}(v)$  alone. Indeed, while  $\sigma_{\text{I}}(v)$  can be easily made to satisfy the condition at  $v = 0$ , see (3.7), it cannot satisfy the one at  $v = 1$ , see (3.9), since the coefficient  $A$ , given by (4.7), has a different  $\alpha$ -dependence. At the same time, function  $\sigma_{\text{II}}(v)$  can be chosen to satisfy the boundary condition at  $v = 1$ , but it cannot be made consistent with the one at  $v = 0$ .

Thus, to satisfy the boundary conditions we have to assume that the function  $\sigma(v)$  is given by a combination of the two solutions above, in agreement with the discussion at the end of Sect. 2, as follows:

$$\sigma(v) = \begin{cases} \sigma_{\text{I}}(v) & v \in [0, v_c] \\ \sigma_{\text{II}}(v) & v \in [v_c, 1]. \end{cases} \quad (4.13)$$

Here  $v_c$  is some function of the parameter  $\alpha$ . As we show in the remaining part of this section, the assumption of the structure of the function  $\sigma(v)$  given by (4.13) allows one to construct the unique solution of (4.1), which possesses the required properties of being a continuous, nonnegative and nondecreasing function of  $v$  over the whole interval  $[0, 1]$ , and satisfies the boundary conditions (3.7) and (3.9).

To completely determine our function  $\sigma(v)$  according to (4.13), and find  $v_c$ , we first satisfy the boundary conditions by fixing the constants  $a_1$ ,  $a_2$ ,  $b_1$ , and  $b_2$  entering (4.6) and (4.8). At  $v = 0$ , see (3.7), we have the condition  $A = 0$ , that is  $a_1 = a_2 = 0$ . Thus, the solution  $\sigma_{\text{I}}(v)$  relevant to our function  $\sigma(v)$  is just

$$\sigma_{\text{I}}(v) = 0. \quad (4.14)$$

Let us now consider the point  $v = 1$ , see (3.9). From (4.8), (4.9) and (4.12) we get

$$\sigma_{\text{II}}(1) = b_1 + b_2 \log \alpha + \log \frac{\sqrt{\alpha}}{1 - \alpha} \quad (4.15)$$

and hence (3.9) can be satisfied by choosing  $b_1 = 0$  and  $b_2 = -1/2$ . The resulting function  $\sigma_{\text{II}}(v)$  can be written as

$$\sigma_{\text{II}}(v) = v^2 \log \frac{v}{u} - \frac{(1-v)^2}{2} \log \frac{1-v}{1-u} - \frac{(1+v)^2}{2} \log \frac{1+v}{1+u}, \quad (4.16)$$

where  $u$  is defined in (4.12).

The value  $v_c$  can now be determined from the requirement that the function  $\sigma(v)$ , given by (4.13), (4.14) and (4.16), is continuous, nonnegative and nondecreasing. Since  $\sigma_{\text{I}}(v)$  is just equal to zero, continuity implies that  $\sigma_{\text{II}}(v_c) = 0$ . From (4.16) one can see that  $\sigma_{\text{II}}(v)$  is positive and monotonously increasing, from 0 at  $v = u$  to its boundary value  $-\log(1 - \alpha)$  at  $v = 1$ . This allows one to determine the value of the constant  $v_c$  in (4.13) to be

$$v_c = u = \frac{1 - \sqrt{\alpha}}{1 + \sqrt{\alpha}}. \quad (4.17)$$

Thus, the function  $\sigma(v)$  is given by (4.13), (4.14), (4.16) and (4.17).

As a simple verification of our result here, one can easily check that the limiting conditions at  $\alpha = 0$  and at  $\alpha = 1$ , given by (3.11) and (3.14), respectively, are indeed satisfied.

### 5. The random matrix model approach

Here we exploit the approach of [29]. We start from representation (3.4), which we write separating explicitly the matrix model integral

$$f_{r,s} = \frac{(1-\alpha)^{s^2}}{\alpha^{s(s-1)/2}} I_{r,s}, \quad (5.1)$$

where we have defined

$$I_{r,s} = \frac{1}{s! \left( \prod_{j=1}^{s-1} j! \right)^2} \sum_{m_1=0}^{r-1} \cdots \sum_{m_s=0}^{r-1} \prod_{j < k} (m_k - m_j)^2 \prod_{j=1}^s \alpha^{m_j}. \quad (5.2)$$

In this formula one can easily recognize the discrete measure analogue of an Hermitian  $s \times s$  random matrix integral in terms of its eigenvalues. Introducing the rescaled coordinate  $R = r/s$ , the large  $s$  limit of  $I_{r,s}$  can be described by the function  $\Phi(R)$ , defined by

$$I_{r,s} = \exp \left\{ s^2 \Phi(r/s) + o(s^2) \right\}, \quad s \rightarrow \infty. \quad (5.3)$$

The functions  $\sigma(v)$ , defined by (2.9), and  $\Phi(R)$  are related by

$$\sigma(v) = -v^2 \log \frac{1-\alpha}{\sqrt{\alpha}} - v^2 \Phi(1/v), \quad (5.4)$$

and variables  $v$  and  $R$  are related by  $v = 1/R$ .

To derive the function  $\Phi(R)$  we rewrite (5.2), introducing the rescaled variables  $\mu_j$  as follows:

$$m_k = s\mu_j, \quad j = 1, \dots, s. \quad (5.5)$$

After rescaling, sums can be reinterpreted as Riemann sums, and in the large  $s$  limit replaced by integrals, so that, as  $s \rightarrow \infty$ ,

$$I_{r,s} \sim \varkappa_s \int_0^R \cdots \int_0^R \prod_{j < k} (\mu_k - \mu_j)^2 \exp \left\{ s \log \alpha \sum_{j=1}^s \mu_j \right\} d^s \mu, \quad (5.6)$$

where the normalization constant  $\varkappa_s$  can be easily inferred from (5.2), but is unessential for what follows.

Now the usual random matrix saddle-point analysis can be applied, provided that one imposes a suitable additional constraint keeping track of the discreteness of the  $m_j$ 's [30], see also [29, 31]. In (5.2), all  $m_j$ 's must be distinct, otherwise the Vandermonde determinant vanishes, and therefore  $|m_k - m_j| \geq 1$ , for all  $j \neq k$ . Introducing the density  $\rho(\mu)$  of the rescaled variables  $\mu_j$ , satisfying the normalization condition

$$\int \rho(\mu) d\mu = 1, \quad (5.7)$$

the constraint simply reads:

$$\rho(\mu) \leq 1. \quad (5.8)$$

In general, when the eigenvalues are trapped in a well of the potential, they accumulate with maximal density at the bottom of the well. In the present situation of discrete eigenvalues, due to (5.8), saturated regions, i.e., where  $\rho(\mu) = 1$ , may arise.

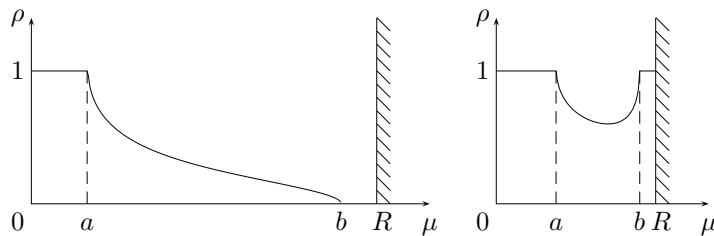


FIGURE 5. Plots of densities in the two scenarios.

Another phenomenon in the present situation is related to the presence of “hard walls”, i.e., the fact that the rescaled eigenvalues are restricted to the interval  $\mu_j \in [0, R]$ . If the eigenvalues were continuous, this would imply, in the case of nonvanishing density near an hard wall, an inverse square root singularity for the density [32–37]. Hence, due to the constraint (5.8) in the case of discrete eigenvalues, in the vicinity of the hard wall the density can only vanish or saturate [38].

In the random matrix model picture (5.6) we have the hard wall potential well  $V(\mu) = +\infty$ , for  $\mu \notin [0, R]$ , and

$$V(\mu) = -\mu \log \alpha, \quad \mu \in [0, R]. \quad (5.9)$$

Note that the potential is linear for  $\mu \in [0, R]$ , with a positive slope, since  $\alpha \in (0, 1)$ .

In view of the previous discussion, it is clear that according to the values of the parameters  $\alpha$  and  $R$  two different scenarios can manifest. Let us start with considering very large values of  $R$  (and some generic fixed value of  $\alpha \neq 0, 1$ ). Since the eigenvalues accumulate to the bottom of the linear potential, a saturated region  $\rho(\mu) = 1$  arises near the origin. At the same time, the wall at  $\mu = R$  is very far on the right and can be ignored. Introducing positive real parameters  $a$  and  $b$ , with  $0 < a < b < R$ , to be determined later, we thus have a saturated region  $\rho(\mu) = 1$  on some interval  $\mu \in [0, a]$ , with an unsaturated region  $\mu \in [a, b]$ , and vanishing eigenvalue density for  $\mu \in [b, R]$ , see Figure 5, picture on the left.

As  $R$  decreases, as far as it remains larger than  $b$ , nothing changes in the previous scenario. But as soon as  $b = R$ , the eigenvalue density is constrained to jump from  $\rho(R) = 0$  to  $\rho(R) = 1$  and a new scenario arises, with a saturated region on some interval  $\mu \in [0, a]$ , an unsaturated region  $\mu \in [a, b]$ , and a second saturated region for  $\mu \in [b, R]$ , see Figure 5, picture on the right.

As  $R$  decreases further and approaches the value  $R = 1$ , the number of available positions becomes smaller and smaller, and eventually barely sufficient to accommodate the  $s$  distinct eigenvalues. Correspondingly, the central unsaturated region of the second scenario shrinks down. In particular, at  $R = 1$ , the central unsaturated region disappears completely, and  $\rho(\mu) = 1$ , for  $\mu \in [0, 1]$ . At the end, there is no admissible eigenvalue configuration for  $R < 1$ .

To proceed, we recall that in the saddle-point approximation the eigenvalue density is related to the resolvent

$$W(z) = \int_S \frac{\rho(\mu)}{z - \mu} d\mu, \quad z \notin S, \quad (5.10)$$

in particular, to its discontinuity across its cut  $S$ ,

$$\rho(z) = -\frac{1}{2\pi i} [W(z + i0) - W(z - i0)], \quad z \in S. \quad (5.11)$$

Clearly,  $S$  is also the support of the density  $\rho(\mu)$ . In turn, the resolvent is determined by the saddle-point equation

$$W(z + i0) + W(z - i0) = U(z), \quad z \in S. \quad (5.12)$$

In the case of a continuous measure,  $U(z)$  is just equal to the derivative  $V'(z)$ , where  $V(z)$  is the potential of the model. However, in the case of discrete measure, this holds only as far as the density  $\rho(z)$  does not saturate the constraint (5.8). The occurrence of saturation in the density requires modifying the form of  $U(z)$  and  $S$  in (5.12), as we shall discuss later on.

Assuming that  $S$  consists of a single interval  $[a, b]$  on the real axis, the solution of (5.12) that is consistent with (5.10) is

$$W(z) = \frac{\sqrt{(z-a)(z-b)}}{2\pi} \int_a^b \frac{U(u)}{(z-u)\sqrt{(u-a)(b-u)}} du, \quad (5.13)$$

Imposing the large  $z$  asymptotic behavior implied by (5.10) together with (5.7), on the order  $z^0$  and  $z^{-1}$  terms of the large  $z$  expansion of (5.13) fixes the endpoints  $a$  and  $b$  of the interval  $S$ .

Denoting by  $E$  the average of the eigenvalues (i.e., the first moment of the density  $\rho(z)$ ), we note that it can be extracted from the order  $z^{-2}$  coefficient,

$$W(z) = \frac{1}{z} + \frac{E}{z^2} + O(z^{-3}), \quad |z| \rightarrow \infty. \quad (5.14)$$

In the case of potential of the form (5.9), the average  $E$  can be related to the function  $\Phi(R)$ , defined in (5.3), by

$$\alpha \partial_\alpha \Phi(R) = E, \quad (5.15)$$

allowing one to determine  $\Phi(R)$  up to some quantity independent of  $\alpha$ .

Now we find solutions  $W_{\text{I}}(z)$  and  $W_{\text{II}}(z)$  of the saddle-point equations corresponding to the two scenarios outlined above, respectively. We also compute the corresponding functions  $\Phi_{\text{I}}(z)$  and  $\Phi_{\text{II}}(z)$ , and show that they indeed reproduce (4.14) and (4.16), as expected.

Let us consider the first scenario, with one saturated region, i.e., with  $\rho(\mu) = 1$ , for  $\mu \in [0, a]$ . The saddle-point problem in this case coincides with that arising in the matrix model associated to the partition function of the domain wall six-vertex model in its ferroelectric phase, see [29], Section 3 (see also [28, 31, 39]). The saturated region in the interval  $[0, a]$  gives rise to a logarithmic cut in the resolvent  $W_{\text{I}}(z)$ , which can be removed by introducing an auxiliary function  $H_{\text{I}}(z)$  as follows:

$$W_{\text{I}}(z) = \log \frac{z}{z-a} + H_{\text{I}}(z). \quad (5.16)$$

The saddle-point equation for  $H_{\text{I}}(z)$  reads

$$H_{\text{I}}(z + i0) + H_{\text{I}}(z - i0) = -2 \log \frac{\sqrt{\alpha} z}{z-a}, \quad z \in [a, b]. \quad (5.17)$$

Exploiting (5.12) and (5.13), and evaluating the resulting integral (see Appendix B), one has:

$$W_{\text{I}}(z) = -\log \sqrt{\alpha} - 2 \log \frac{\sqrt{a(z-b)} + \sqrt{b(z-a)}}{\sqrt{(b-a)z}}. \quad (5.18)$$

Imposing the asymptotic behavior (5.14) provides the conditions

$$\frac{\sqrt{b} - \sqrt{a}}{\sqrt{b} + \sqrt{a}} = \sqrt{\alpha}, \quad \sqrt{ab} = 1, \quad (5.19)$$

with the solution

$$a = \frac{1 - \sqrt{\alpha}}{1 + \sqrt{\alpha}}, \quad b = \frac{1 + \sqrt{\alpha}}{1 - \sqrt{\alpha}}. \quad (5.20)$$

Recall that the scenario holds as long as  $R > R_c$ . The critical value  $R_c$ , at which the transition to the the second scenario takes place, corresponds to  $R_c = b$ , where the value for  $b$  is given above. Hence,

$$R_c = \frac{1 + \sqrt{\alpha}}{1 - \sqrt{\alpha}}. \quad (5.21)$$

Recalling that  $v = 1/R$ , this obviously reproduces (4.17).

To conclude the discussion of the first scenario, we evaluate the function  $\Phi_I(R)$ . Expanding (5.18) up to the order  $z^{-2}$ , we get

$$E_I = \frac{a + b}{4} = \frac{1 + \alpha}{2(1 - \alpha)}. \quad (5.22)$$

Integration yields

$$\Phi_I(R) = \log \frac{\sqrt{\alpha}}{1 - \alpha}, \quad (5.23)$$

where the integration constant is fixed to comply with the condition (3.11). As a result, see (5.4), we reproduce (4.14).

Let us now turn to the second scenario, with two saturated regions, i.e., with  $\rho(\mu) = 1$ , for  $\mu \in [0, a] \cup [b, R]$ . We first remove the logarithmic cuts of  $W_{II}(z)$  arising from the saturated regions,

$$W_{II}(z) = \log \frac{z(z - b)}{(z - a)(z - R)} + H_{II}(z). \quad (5.24)$$

The saddle-point equation for  $H_{II}(z)$  reads

$$H_{II}(z + i0) + H_{II}(z - i0) = -2 \log \frac{\sqrt{\alpha} z(z - b)}{(z - a)(z - R)}, \quad z \in [a, b]. \quad (5.25)$$

Using (5.13), and evaluating the resulting integral (see Appendix B), we obtain

$$W_{II}(z) = -\log \sqrt{\alpha} - \log \frac{z - R}{z} - 2 \log \frac{\sqrt{a(z - b)} + \sqrt{b(z - a)}}{\sqrt{R - a}\sqrt{z - b} + \sqrt{R - b}\sqrt{z - a}}. \quad (5.26)$$

Imposing the asymptotic behavior (5.14) we obtain the two conditions,

$$\begin{aligned} \left( \frac{\sqrt{R - a} + \sqrt{R - b}}{\sqrt{b} + \sqrt{a}} \right)^2 &= \sqrt{\alpha}, \\ \sqrt{ab} + \sqrt{(R - a)(R - b)} &= 1, \end{aligned} \quad (5.27)$$

with the solution

$$a = \frac{(\sqrt{R + 1} - \sqrt{(R - 1)\sqrt{\alpha}})^2}{2(1 + \sqrt{\alpha})}, \quad b = \frac{(\sqrt{R + 1} + \sqrt{(R - 1)\sqrt{\alpha}})^2}{2(1 + \sqrt{\alpha})}. \quad (5.28)$$

The critical value  $R_c$ , which corresponds to the case  $b = R$ , reproduces (5.21), as it should.

Now we are ready to compute the function  $\Phi_{\text{II}}(R)$ . Calculation of the  $z^{-2}$  order term in the large  $z$  expansion of (5.26) provides the first moment of the eigenvalue density:

$$E_{\text{II}} = \frac{a+b}{4} + \frac{R}{2} \sqrt{(R-a)(R-b)}. \quad (5.29)$$

Substituting here  $a$  and  $b$  from (5.28), and integrating (5.15), we obtain the expression

$$\Phi_{\text{II}}(R) = (R^2 - 1) \log \frac{1 + \sqrt{\alpha}}{2\alpha^{1/4}} + R \log \sqrt{\alpha} + C(R). \quad (5.30)$$

Here the integration constant  $C(R)$ , a quantity independent of  $\alpha$ , can be determined due to the condition (3.14), with the result  $C(R) = -R^2\psi(1/R)$ . Recalling (5.4), it is immediately seen that (5.30) indeed reproduces the result of the previous section, (4.16), for the function  $\sigma(v)$ .

## 6. Discussion

Let us first summarize the results. Our main result concerns the explicit form of the function  $\sigma(v)$ , describing the thermodynamic limit behavior of EFP. In deriving this result we used two different methods. The first method is based on the connection of the Hankel determinant representation for EFP with Toda chain differential equations, and allows one to derive the result by rather elementary means. The second method exploits the fact that the Hankel determinant can be represented as a random matrix model integral. An unusual feature of the matrix model arising in our study is the presence of a discrete measure on a finite interval.

For the function  $\sigma(v)$  we have derived the following expression:

$$\sigma(v) = \begin{cases} 0 & v \in [0, v_c] \\ v^2 \log \frac{v}{v_c} - \frac{(1-v)^2}{2} \log \frac{1-v}{1-v_c} - \frac{(1+v)^2}{2} \log \frac{1+v}{1+v_c} & v \in [v_c, 1]. \end{cases} \quad (6.1)$$

The critical value  $v_c = v_c(\alpha)$ , at which function  $\sigma(v)$  changes its behavior is

$$v_c = \frac{1 - \sqrt{\alpha}}{1 + \sqrt{\alpha}}. \quad (6.2)$$

The formulas above show that  $\sigma'(v)$  and  $\sigma''(v)$ , where the prime denotes derivative, are continuous functions in the vicinity of  $v = v_c$ , with the values  $\sigma'(v_c) = \sigma''(v_c) = 0$ , while the third derivative has a discontinuity, since

$$\lim_{v \searrow v_c} \sigma'''(v) = \frac{1}{v_c(1-v_c^2)}. \quad (6.3)$$

Thus at  $v = v_c$  the function  $F(v)$ , which is the free energy per domino for the domino tilings of the Aztec diamond with a cut-off corner, has a discontinuity in its third derivative, i.e., at  $v = v_c$  the model undergoes a third-order phase transition with respect to the scaled size of the cut-off corner.

Let us now discuss the results. We first point out the meaning of the change of the behavior of the function  $\sigma(v)$  at  $v = v_c$ . The value  $v = v_c$  has a simple interpretation in terms of the original model, i.e. the unmodified Aztec diamond, where frozen and temperate regions are separated by the so-called arctic ellipse,

$$\frac{(1-x-y)^2}{\alpha} + \frac{(x-y)^2}{1-\alpha} = 1. \quad (6.4)$$



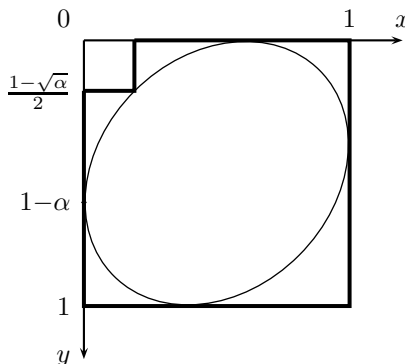


FIGURE 6. A meaning of  $v_c$ : the cut off corner hits the arctic ellipse of the initial Aztec diamond,  $v_c/(1 + v_c) = (1 - \sqrt{\alpha})/2$ .

The value of  $v_c$  given by (6.2) exactly corresponds to the situation in which the cut-off corner, increasing in size, gets large enough to reach the arctic ellipse of the original (unmodified) Aztec diamond, see Figure 6.

This result suggests to view the phase separation curves as critical curves in the space of parameters describing the macroscopic geometry of the tiled region. Indeed, while here we have restricted ourselves to the case of a square shaped cut-off corner, one could consider the more general situation of a rectangular shaped cut-off corner. The treatment is essentially the same, with the free energy now exhibiting a whole critical line, which coincides with the full portion of the ellipse (6.4) between its contact points with the top and left boundaries. While finding the critical curve is straightforward, the evaluation of the free energy is more involved, and will be reported elsewhere.

Coming back to the discussion of a third-order phase transition in random tilings, (6.1) can also be interpreted in a slightly different manner, treating the size of the cut-off corner as some given parameter, fixed from the beginning. Then, changing the Boltzmann weights, that is varying the parameter  $\alpha$ , we again have a third-order phase transition, as it can be easily verified from (6.1), when the ellipse, deforming itself as  $\alpha$  is increasing, reaches the bottom-right vertex of the cut-off corner.

Recalling that the parameter  $\alpha$  tunes the asymmetry between the two possible orientations of dominoes, we see that the last interpretation regards the arctic curves as critical curves in the space of external fields acting on the system. A similar point of view has already been considered, e.g., in the six-vertex model, where the limit shape of the system has equivalently been studied in the space parameterized by some external electric fields acting on it [40].

Interestingly enough, besides random tilings, this interpretation may also have implications in the context of quantum spin chains, in view of the well-known relation between the six-vertex model and the 1D quantum Heisenberg spin chain. Remnants of the arctic phenomena can be seen when EFP of the quantum spin chain is treated by conformal field theory methods [41]. A possible third-order phase transition in the quantum spin chain, although for a very peculiar choice of the macroscopic parameters, has been pointed out recently in [42]. Third-order

phase transitions have also been observed in the related context of vicious walkers [43].

Our last comment here concerns the observed phase transition from the point of view of the random matrix model description. In this respect we recall two other third-order phase transitions related to random matrix models, namely the Gross-Witten-Wadia [44, 45], and the Douglas-Kazakov [30] phase transitions, occurring in the large  $N$  limit of  $U(N)$  Yang-Mills theory in two dimensions, when formulated on the lattice, or in the continuum, respectively.

From the point of view of the random matrix model picture, in the Gross-Witten-Wadia transition, the eigenvalues live on the unit circle, and the two phases correspond to the support of the eigenvalue density extending to the whole circle, or being restricted to an arc. In the Douglas-Kazakov transition the eigenvalues are discrete, thus imposing an upper limit on the eigenvalue density. The two phases correspond to the presence or absence of saturation in the eigenvalue density.

The matrix model phase transition observed here in relation to random tilings shares properties with both Gross-Witten-Wadia and Douglas-Kazakov phase transitions. Indeed, the transition can be attributed to the rise of a saturated region, just like in the Douglas-Kazakov transition. At the same time, the two phases correspond to the support of the eigenvalue density extending to the whole allowed interval for the eigenvalues or restricting to a subset of it, like in the Gross-Witten-Wadia transition. We note further that a common feature of these transitions is that they all correspond to the appearance or disappearance of some edge of the support of the (unsaturated part of the) eigenvalue density. The order of the transition can be ascribed to the square-root behaviour of the density at these edges.

In conclusion, we have discussed a third-order phase transition arising in the random tilings of the Aztec diamond with a cut-off corner, by deriving the leading term of asymptotics of a particular correlation function in the closely related case of the six-vertex model. While here we have considered only the domino tilings of the Aztec diamond with a cut-off corner, we believe that the phenomenon is rather universal, and may be observed similarly in other tiling problems where the phase separation phenomena are known to take place, e.g., in the rhombus tilings of an hexagon with a cut-off rhombus, and many others.

### Acknowledgments

We are indebted to A. Kuijlaars and N. Reshetikhin for useful discussions. This work is partially supported by the IRSES grant of EC-FP7 Marie Curie Action ‘‘Quantum Integrability, Conformal Field Theory and Topological Quantum Computation’’ (QIFCT). A.G.P. acknowledges partial support from the Russian Foundation for Basic Research (grant 13-01-00336) and from INFN, Sezione di Firenze.

### Appendix A. Evaluation of determinants

Here we outline the evaluation of two determinants used in Section 3. Namely, the determinant in (3.1) admits explicit factorized expressions in the two cases:  $r = \infty$ , at arbitrary  $\alpha$ , and  $\alpha = 1$ , at arbitrary  $r$ .

In the first case,  $r = \infty$ , the entries of the determinant in (3.1) can be recognized as the moments of the orthogonality measure of Meixner polynomials  $M_j(m; 1, \alpha)$ ; for notation and summary of properties we refer to [46], Section 9.10. Hence, we can

regard the determinant in (3.1) at  $r = \infty$  as the Gram determinant of the Meixner polynomials, equal to  $\prod_{j=0}^{s-1} h_j / \kappa_j^2$ , where  $h_j$  and  $\kappa_j$  are the square norm and the leading coefficient of the polynomial  $M_j(m; 1, \alpha)$ . Using the known expressions

$$h_j = \frac{1}{(1-\alpha)\alpha^j}, \quad \kappa_j = \frac{(\alpha-1)^j}{j!\alpha^j}, \quad (\text{A.1})$$

we can evaluate the determinant, with the result:

$$\det_{1 \leq j < k \leq s} \left[ \sum_{m=0}^{\infty} m^{j+k-2} \alpha^m \right] = \prod_{j=0}^{s-1} \frac{(j!)^2 \alpha^j}{(1-\alpha)^{2j+1}}. \quad (\text{A.2})$$

This expression allows estimating the large  $r$  behavior of the determinant in (3.1), at fixed  $s$ , see (3.6).

In the second case,  $\alpha = 1$ , the determinant in (3.1) can be similarly recognized as the Gram determinant of Hahn polynomials  $Q_j(m; 0, 0, r-1)$ , see [46], Section 9.5. The square norm and the leading coefficient are

$$h_j = \frac{(j+r)!(r-j-1)!}{(2j+1)((r-1)!)^2}, \quad \kappa_j = (-1)^j \frac{(2j)!(r-j-1)!}{(j!)^2(r-1)!}. \quad (\text{A.3})$$

Hence,

$$\det_{1 \leq j < k \leq s} \left[ \sum_{m=0}^{r-1} m^{j+k-2} \right] = \prod_{j=0}^{s-1} \frac{(j!)^4 (j+r)!}{(2j)!(r-j-1)!(2j+1)!}. \quad (\text{A.4})$$

This leads immediately to expression (3.13) for the quantity  $C_{r,s}$ , which, in turn, gives rise to the function  $\psi(v)$ , see (3.15) and (3.16).

## Appendix B. Resolvents and eigenvalue densities

Here we explain the origin of (5.18) and (5.26), and provide the explicit expression for the eigenvalue densities associated to the two scenarios appearing in the study of the random matrix integral (5.6).

The explicit solution of the saddle-point equations (5.17) and (5.25) is given by the integral (5.13) by suitably specifying the function  $U(z)$ . In this way we obtain expressions for the functions  $H_{\text{I}}(z)$  and  $H_{\text{II}}(z)$ , which, when substituted in (5.16) and (5.24), give rise to (5.18) and (5.26), respectively. The appearing integrals can be evaluated using

$$\begin{aligned} & \int_a^b \frac{1}{(z-u)\sqrt{(u-a)(b-u)}} \log \frac{u-c}{u-d} du \\ &= \begin{cases} \frac{2\pi}{\sqrt{(z-a)(z-b)}} \log \frac{\sqrt{a-c}\sqrt{z-b} + \sqrt{b-c}\sqrt{z-a}}{\sqrt{a-d}\sqrt{z-b} + \sqrt{b-d}\sqrt{z-a}} & (c, d \leq a) \\ \frac{2\pi}{\sqrt{(z-a)(z-b)}} \log \frac{\sqrt{c-a}\sqrt{z-b} + \sqrt{c-b}\sqrt{z-a}}{\sqrt{d-a}\sqrt{z-b} + \sqrt{d-b}\sqrt{z-a}} & (c, d \geq b) \end{cases} \quad (\text{B.1}) \end{aligned}$$

which holds for  $z \in \mathbb{C} \setminus [a, b]$ .

Explicit expressions for the eigenvalue densities corresponding to the two scenarios can be extracted from the resolvents using (5.11). In the first scenario, the resolvent  $W_{\text{I}}(z)$  has the form (5.18), leading to

$$\rho_{\text{I}}(z) = \frac{2}{\pi} \arctan \frac{\sqrt{a(b-z)}}{\sqrt{b(z-a)}}, \quad z \in [a, b]. \quad (\text{B.2})$$

Recall that  $\rho_{\text{I}}(z) = 1$  for  $z \in [0, a]$ , and  $\rho_{\text{I}}(z) = 0$  for  $z \in [b, R]$ .

In the second scenario, the resolvent  $W_{\text{II}}(z)$  has the form (5.26), and (5.11) gives

$$\rho_{\text{II}}(z) = \frac{2}{\pi} \arctan \frac{\sqrt{a(b-z)}}{\sqrt{b(z-a)}} - \frac{2}{\pi} \arctan \frac{\sqrt{(R-a)(b-z)}}{\sqrt{(R-b)(z-a)}} + 1, \quad z \in [a, b] \quad (\text{B.3})$$

with  $\rho_{\text{II}}(z) = 1$  for  $z \in [0, a] \cup [b, R]$ .

As an example, Figure 5 shows plots of the eigenvalue densities in the case of  $\alpha = 0.25$ , in which  $R_c = 3$ , for some  $R > 3$  and for  $R = 1.2$ , corresponding to the first and the second scenario, respectively.

## References

- [1] H. N. V. Temperley and M. E. Fisher, *The dimer problem in statistical mechanics—an exact result*, *Phyl. Mag.* **6** (1961), 1061–1663.
- [2] M. E. Fisher, *Statistical mechanics of dimers on a plane lattice*, *Phys. Rev.* **124** (1961), 1664–1672.
- [3] P. W. Kasteleyn, *The statistics of dimers on a lattice. I. The number of dimer arrangements on a quadratic lattice*, *Physica* **27** (1961), 1209–1225.
- [4] P. W. Kasteleyn, *Dimer statistics and phase transitions*, *J. Math. Phys.* **4** (1963), 287–297.
- [5] W. T. Lu and F. Y. Wu, *Dimer statistics on the Moebius strip and the Klein bottle*, *Phys. Lett. A* **259** (1999), 108–114.
- [6] J. P. Garrahan, A. Stannard, M. O. Blunt, and P. H. Beton, *Molecular random tilings as glasses*, *Proc. Natl. Acad. Sci. USA* **106** (2009), 15209–15213, arXiv:0903.1551.
- [7] S. Whitelam, I. Tamblyn, P. H. Beton, and J. P. Garrahan, *Random and ordered phases of off-lattice rhombus tiles*, *Phys. Rev. Lett.* **108** (2012), 035702, arXiv:1109.1450.
- [8] W. Jockush, J. Propp, and P. Shor, *Random domino tilings and the arctic circle theorem*, arXiv:math/9801068.
- [9] S. Chhita, K. Johansson, and B. Young, *Asymptotic domino statistics in the Aztec diamond*, arXiv:1212.5414.
- [10] H. Cohn, M. Larsen, and J. Propp, *The shape of a typical boxed plane partition*, *New York J. Math.* **4** (1998), 137–165, arXiv:math/9801059.
- [11] R. Kenyon and A. Okounkov, *Limit shapes and the complex Burgers equation*, *Acta Math.* **199** (2007), 263–302, arXiv:math-ph/0507007.
- [12] R. Kenyon, A. Okounkov, and S. Sheffield, *Dimers and amoebae*, *Ann. of Math.* **163** (2006), 1019–1056, arXiv:math-ph/0311005.
- [13] R. Kenyon and A. Okounkov, *Planar dimers and Harnack curves*, *Duke Math. J.* **131** (2006), 499–524, arXiv:math-ph/0311005.
- [14] K. Eloranta, *Diamond ice*, *J. Stat. Phys.* **96** (1999), 1091–1109.
- [15] O. F. Syljuåsen and M. B. Zvonarev, *Monte-Carlo simulations of vertex models*, *Phys. Rev. E* **70** (2004), 016118, arXiv:cond-mat/0401491.
- [16] D. Allison and N. Reshetikhin, *Numerical study of the 6-vertex model with domain wall boundary conditions*, *Ann. Inst. Fourier (Grenoble)* **55** (2005), 1847–1869, arXiv:cond-mat/0502314.
- [17] F. Colomo and A. G. Pronko, *The limit shape of large alternating-sign matrices*, *SIAM J. Discrete Math.* **24** (2010), 1558–1571, arXiv:0803.2697.
- [18] F. Colomo and A. G. Pronko, *The arctic curve of the domain-wall six-vertex model*, *J. Stat. Phys.* **138** (2010), 662–700, arXiv:0907.1264.
- [19] F. Colomo, A. G. Pronko, and P. Zinn-Justin, *The arctic curve of the domain-wall six-vertex model in its anti-ferroelectric regime*, *J. Stat. Mech. Theory Exp.* (2010), L03002, arXiv:1001.2189.
- [20] V. E. Korepin, *Calculations of norms of Bethe wave functions*, *Comm. Math. Phys.* **86** (1982), 391–418.
- [21] N. Elkies, G. Kuperberg, M. Larsen, and J. Propp, *Alternating-sign matrices and domino tilings*, *J. Algebraic Combin.* **1** (1992), 111–132; 219–234.
- [22] F. Colomo and A. G. Pronko, *Emptiness formation probability in the domain-wall six-vertex model*, *Nucl. Phys. B* **798** (2008), 340–362, arXiv:0712.1524.

- [23] N. M. Bogoliubov, A. V. Kitaev, and M. B. Zvonarev, *Boundary polarization in the six-vertex model*, Phys. Rev. E **65** (2002), 026126, arXiv:cond-mat/0107146.
- [24] F. Colomo and A. G. Pronko, *The Arctic Circle revisited*, Contemp. Math. **458** (2008), 361–376, arXiv:0704.0362.
- [25] A. G. Pronko, *On the emptiness formation probability in the free-fermion six-vertex model with domain wall boundary conditions*, J. Math. Sci. (N. Y.) **192** (2013), 101–116.
- [26] H. Au-Yang and J. H. H. Perk, *Critical correlations in a Z-invariant inhomogeneous Ising model*, Physica A **144** (1987), 44–104.
- [27] V. E. Korepin and P. Zinn-Justin, *Thermodynamic limit of the six-vertex model with domain wall boundary conditions*, J. Phys. A **33** (2000), 7053–7066, arXiv:cond-mat/0004250.
- [28] K. Johansson, *Shape fluctuations and random matrices*, Comm. Math. Phys. **209** (2000), 437–476, arXiv:math/9903134.
- [29] P. Zinn-Justin, *Six-vertex model with domain wall boundary conditions and one-matrix model*, Phys. Rev. E **62** (2000), 3411–3418, arXiv:math-ph/0005008.
- [30] M.R. Douglas and V.A. Kazakov, *Large N phase transition in continuum QCD<sub>2</sub>*, Phys. Lett. B **319** (1993), 219–230.
- [31] E. Brezin and V. Kazakov, *Universality of correlations of levels with discrete statistics*, Comm. Math. Phys. **214** (2000), 233–247.
- [32] B.V. Bronk, *Exponential ensemble for random matrices*, J. Math. Phys. **6** (1965), 228.
- [33] T. Nagao and M. Wadati, *Correlation functions of random matrix ensembles related to classical orthogonal polynomials*, J. Phys. Soc. Japan **60** (1991), 3298–3322.
- [34] C. A. Tracy and H. Widom, *Level spacing distributions and the Bessel kernel*, Comm. Math. Phys. **161** (1994), 289–309, arXiv:hep-th/9304063.
- [35] D. S. Dean and S. N. Majumdar, *Large deviations of extreme eigenvalues of random matrices*, Phys. Rev. Lett. **97** (2006), 160201, arXiv:cond-mat/0609651.
- [36] D. S. Dean and S. N. Majumdar, *Extreme value statistics of eigenvalues of gaussian random matrices*, Phys. Rev. E **77** (2008), 041108, arXiv:0801.1730.
- [37] T. Claeys and A. B. J. Kuijlaars, *Universality in unitary random matrix ensembles when the soft edge meets the hard edge*, Contemp. Math. **458** (2008), 265–280, arXiv:math-ph/0701003.
- [38] P. D. Draznev and E. B. Saff., *A problem in potential theory and zero asymptotics of Krautchouk polynomials*, J. Approx. Theory **102** (2000), 120–140.
- [39] P. Bleher and K. Liechty, *Exact solution of the six-vertex model with domain wall boundary conditions. Ferroelectric phase*, Comm. Math. Phys. **286** (2009), 777–801, arXiv:0711.4091.
- [40] N. Reshetikhin and K. Palamarchuk, *The 6-vertex model with fixed boundary conditions*, PoS Solvay (2006), 012, arXiv:cond-mat/0502314.
- [41] J.-M. Stéphan, *Emptiness formation probability, Toeplitz determinants, and conformal field theory*, arXiv:1303.5499.
- [42] D. Pérez-García and M. Tierz, *The Heisenberg XX spin chain and low-energy QCD*, arXiv:1305.3877.
- [43] G. Schehr, S. N. Majumdar, A. Comtet, and P. J. Forrester, *Reunion probability of N vicious walkers: typical and large fluctuations for large N*, J. Stat. Phys. **150** (2013), 491–530, arXiv:1210.4438.
- [44] D. J. Gross and E. Witten, *Possible third-order phase transition in the large-N lattice gauge theory*, Phys. Rev. D **21** (1980), 446–453.
- [45] S. R. Wadia, *N = ∞ phase transition in a class of exactly soluble model lattice gauge theories*, Phys. Lett. B **93** (1980), 403–410.
- [46] R. Koekoek, R. F. Swarttouw, and P. A. Lesky, *Hypergeometric orthogonal polynomials and their q-analogues*, Springer Monographs in Mathematics, Springer-Verlag, Berlin, 2010.

INFN, SEZIONE DI FIRENZE, VIA G. SANSONE 1, 50019 SESTO FIORENTINO (FI), ITALY  
 E-mail address: colomo@fi.infn.it

ST. PETERSBURG DEPARTMENT OF V. A. STEKLOV MATHEMATICAL INSTITUTE OF THE RUSSIAN  
 ACADEMY OF SCIENCES, FONTANKA 27, 191023 ST. PETERSBURG, RUSSIA  
 E-mail address: agp@pdmi.ras.ru